Photodissociation and Electronic Spectroscopy of $[Re(H)(CO)_3(H\text{-}dab)]$ (H-dab = 1,4-diaza-1,3-butadiene): Quantum Wavepacket Dynamics Based on Ab Initio Potentials

Isabelle Bruand-Cote and Chantal Daniel*[a]

Abstract: The photodissociation dynamics of $[Re(H)(CO)_3(H\text{-}dab)]$ (H-dab = 1,4-diaza-1,3-butadiene) were studied by means of wavepacket propagations on CASSCF/MR-CCI potentials calculated for the electronic ground state and low-lying excited states as a function of two coordinates, q_a and q_b, that correspond to the Re–H bond homolysis and to the axial CO loss, respectively. The theoretical absorption spectrum is characterized by two bands, one intense peak centered at $\lambda = 500$ nm (21 000 cm^{-1}) and one broad band centered at 310 nm (32 500 cm^{-1}). The visible band was assigned to the low-lying metal-to-ligand charge-transfer (MLCT) states with a main contribution of the $a^1A' \rightarrow c^1A'$ transition corresponding to the $3d_{xz} \rightarrow \pi^*_{dab}$ excitation. The second band calculated in the UV energy domain was assigned to the d^1A' ($\sigma_{Mn-H} \rightarrow \pi^*_{dab}$) state corresponding to a sigma-bond-to-ligand charge-transfer (SBLCT) state. The photodissociation dynamics of the low-lying ^{1}MLCT and ^{3}SBLCT states following irradiation in the visible energy domain was simulated by wavepacket propagation on the two-dimensional diabatic potentials $V(q_a, q_b)$ coupled by the spin-orbit. In contrast to what was found for the manganese analogue, the ^{1}MLCT state is nonreactive and a rather slow (beyond the ps time scale), nontotal and indirect homolysis of the Re–H bond occurs through ^{1}MLCT $\rightarrow$ ^{3}SBLCT intersystem crossing.

Keywords: ab initio calculations · dynamics · organometallics · photochemistry · quantum chemistry · rhenium

Introduction

Recent experimental studies[1–8] of the $[MR(CO)_3(\alpha\text{-diimine})]$ complexes (in which M = Mn, Re, and R represents a metal fragment, alkyl, or halide groups bound to the metal by a high-lying σ_{M-R} orbital) point to a variety of deactivation mechanisms after irradiation in the visible region ($\lambda = 500$ nm) depending on the metal center, on the nature of the radical R, and on the type of α-diimine ligand. The photochemical reactions currently observed for manganese complexes are either homolytic rupture of the Mn – R bond [Eq. (1)] or carbonyl loss [Eq. (2)].

$$[M(R)(CO)_3(\alpha\text{-diimine})] \xrightarrow{h\nu} R^{\cdot} + [^{\cdot}M(CO)_3(\alpha\text{-diimine})] \quad (1)$$

$$[M(R)(CO)_3(\alpha\text{-diimine})] \xrightarrow{h\nu} [M(R)(CO)_2(\alpha\text{-diimine})] + CO \quad (2)$$

In contrast, the photochemistry of the rhenium complexes is characterized by selective formation of radicals [Eq. (1)]. The rich photochemistry of this class of molecules, caused by electronic delocalization effects over the three chemical centers determined by the metal atom, the α-diimine group and the R ligand, leads to a variety of important applications, such as formation of very unstable unsaturated species used in subsequent catalytic or chemical processes or of radicals initiators of polymerization. Moreover, the presence of long-lived excited state precursors of electron/energy-transfer processes is responsible for intense emissions observed in the rhenium compounds. The quantum yield ϕ of the Re–R bond homolysis may vary between 10^{-2} (R = Me) and ≈ 1.0 (R = ethyl or benzyl).[4–6] A recent femtosecond time-resolved visible absorption study of $[Re(R)(CO)_3(dmb)]$ (dmb = 4,4′-dimethyl-2,2′-bipyridyl) in solution points to an ultrafast (< 400 fs for R = methyl; 600 – 800 fs for R = ethyl) branching between the homolysis of the Re–R bond and relaxation to a low-lying triplet state. According to these experiments, the $Re-CH_3$ bond is cleaved along a single ultrafast pathway with a quantum yield of 0.4 (ϕ_{Re-CH_3}), whereas the homolysis of the $Re-CH_2CH_3$ bond ($\phi Re^-_{CH_2CH_3} = 1.0$) follows two channels corresponding to the ultrafast decay and to a delayed one through a low-lying ^{3}MLCT (≈ 200 ps).[9]

In an attempt to rationalize the experimental data, several theoretical studies, based either on accurate CASSCF/MR-

[a] C. Daniel, I. Bruand-Cote
Laboratoire de Chimie Quantique UMR 7551 CNRS
Université Louis Pasteur, Institut Le Bel
4 Rue Blaise Pascal, 67000 Strasbourg (France)
Fax: (+33) 3-90241589
E-mail: daniel@quantix.u-strasbg.fr

CCI calculations[10–13] and variation of the ligands R and the metal center or on a density functional theory (DFT) approach,[14–16] have been undertaken. The first complete quantum-chemical study of the photodissociation dynamics has been reported for[Mn(H)(CO)$_3$(H-dab)] (H-dab = 1,4-diaza-1,3-butadiene),[17] a model for a broad class of organometallic α-diimine complexes. It has been shown that after irradiation in the visible region to one of the low-lying MLCT states, [Mn(H)(CO)$_3$(H-dab)] dissociates entirely on an ultrafast time scale (less than 500 fs) to the primary products CO + [Mn(H)(CO)$_2$(H-dab)]. The alternative deactivation mechanism, namely an indirect homolytic cleavage of the Mn–H bond through the dissociative ^{3}SBLCT state through intersystem crossing is not competitive with this direct reaction.

To compare the electronic spectra and the photoreactivity of the manganese and rhenium MLCT complexes and to understand the role of the central metal atom, we present here a complete quantum-chemical study of the photodissociation dynamics of [Re(H)(CO)$_3$(H-dab)], as a model complex for a variety of α-diimine organometallic compounds studied for their versatile photochemical/photophysical properties.[1–8] Our aim is to propose a semiquantitative deactivation mechanism of the molecule after visible irradiation. This numerical simulation is based on the two-dimensional CASSCF/MR-CI potential energy surfaces (PES) calculated for the electronic ground state and the lowest excited states as a function of the Re–H and Re–CO$_{ax}$ bond elongations. The excited state dynamics are investigated by means of wavepacket propagations on these PES.

Computational Methods

Quantum-chemical calculations: The calculations were carried out under the C_s symmetry constraint starting from an idealized geometry depicted in Figure 1 for the a^{1}A′ electronic ground state corresponding to the $(\sigma_{Re-H})^2(5d_{x^2-y^2})^2(5d_{yz})^2(5d_{xz})^2$ electronic configuration and for the low-lying ^{1,3}A′ and ^{1,3}A″ MLCT and SBLCT excited states corresponding to 3d → $\pi^*_{H\text{-}dab}$ and $\sigma_{Re-H} \rightarrow \pi^*_{H\text{-}dab}$ excitations, respectively. Idealized geometries were deduced from the ground state structures of [Re(Me)(CO)$_3$(*i*Pr-dab)][18] with the following bond lengths and bond angles: Re–CO 2.00, Re–N 2.177, N–C 1.280, C–C 1.508, N–H 1.010, C–H 1.080 Å; the angles τ, θ and α were kept constant at 96.3, 97.21, and 113.1°, respectively. The Re–H bond length was taken from the experimental structure of [HRe(CO)$_5$][19] (Re–H 1.799 Å).

Gradient/CASSCF optimizations were performed for the electronic ground state and a few excited states: the lowest a^{3}A′ MLCT state corresponding to the $5d_{xz} \rightarrow \pi^*_{H\text{-}dab}$ excitation and the b^{1}A′ state corresponding to $5d_{x^2-y^2} \rightarrow \pi^*_{H\text{-}dab}$ excitation. Convergence problems stopped our attempt to optimise the c^{1}A′ MLCT state corresponding to the $5d_{xz} \rightarrow \pi^*_{H\text{-}dab}$ excitation and the c^{3}A′ SBLCT state corresponding to the $\sigma_{Re-H} \rightarrow \pi^*_{H\text{-}dab}$ excitation. The study of the molecule deformation on going from the electronic ground state to the excited states was the purpose of these calculations. The electronic states and the two-dimensional PES $V(q_a,q_b)$ with q_a = [Re–H] and q_b = [Re–CO$_{ax}$], under the C_s symmetry constraint (Scheme 1) (see the Results section for the choice of coordinates) were obtained by means of complete active space SCF (CASSCF) calculations supplemented by a multireference contracted configuration interaction MR-CCI treatment.

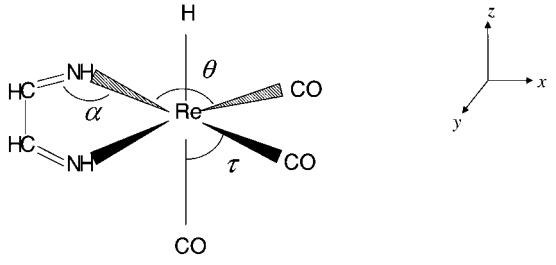

Figure 1. Idealized structure of [Re(H)(CO)$_3$(H-dab)].

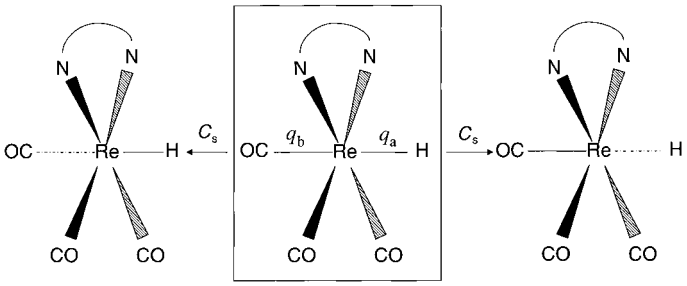

Scheme 1.

Since our interest is centerd mostly on excited states of [Re(H)(CO)$_3$(H-dab)] corresponding to 5d → $\pi^*_{H\text{-}dab}$, 5d → 5d and $\sigma_{Re-H} \rightarrow \pi^*_{H\text{-}dab}$ excitations in the principal configuration, the CASSCF active space is limited to the 5d occupied orbitals of Re and the 5d orbitals which correlate them, the bonding σ_{Re-H} and antibonding σ^*_{Re-H} orbitals involved in the Re–H bond and the low-lying $\pi^*_{H\text{-}dab}$ orbital. Eight electrons were correlated in ten active orbitals in these 8 e10 a CASSCF calculations averaged over seven roots (of equal weights) of a given spin and a given symmetry (^{1,3}A′ and ^{1,3}A″). However, our attempt to introduce the vacant 5d orbital into the active space in order to calculate the metal-centered (MC) states corresponding to 5d → 5d excitations failed. For each electronic state, multireference CCI calculations were carried out, including all the configurations that appear with coefficients larger than 0.08 in the CASSCF expansion, by correlation of eight electrons and including single and double excitations to all virtual orbitals, except the counterparts of the rhenium 6s and 5p orbitals. The accuracy of this computational strategy was tested and discussed for several transition metal complexes investigated for their photochemical properties and compared with reference CASPT2 results in the present work (see next section) and in a number of cases.[17, 20–21] Moreover, comparison with experimental data points to a general agreement with an uncertainty not greater than 1500 cm^{-1}, which is reasonable with regards to the resolution of absorption spectra in organometallic compounds.

Relativistic ECP (effective core potentials in the small core approximation) with the following valence basis sets were used: for the Re center (Z = 15.0), a (8s, 7p, 6d) set contracted to [6s, 5p, 3d],[22] for the C atoms (Z = 4.0) and N atoms (Z = 5.0) a (4s, 4p) set contracted to [2s, 2p], for the O atoms (Z = 6.0) a (4s, 5p) set contracted to [2s, 3p],[23] for the H linked to the metal center a (6s, 1p) set contracted to [3s, 1p] and for the other H atoms, a (4s) set contracted to [2s].[24]

The CASSCF/MR-CCI calculations were performed with the MOLCAS-3 and MOLCAS-4 quantum chemistry software.[25] The electronic dipole transition moments were estimated at the CASSCF level. The spin-orbit coupling between the singlet and the triplet states were evaluated with a restricted full CI scheme and an effective one-electron SO operator operating on the metal center in the L–S coupling scheme.[26] Since only the first derivative part of the kinetic coupling is needed in our approach to the non-adiabatic effects, the kinetic coupling around avoided crossings was approximated by Lorentzians in order to avoid fastidious numerical differentiation of the electronic CASSCF wavefunctions.[27] A few DFT (B3LYP)[28] optimizations were performed for the electronic ground state by the use of either the same ECP and associated basis sets or the LANL2DZ with D95 on first-row atoms[29] and Los Alamos ECP plus Double-ξ on the Re atom[30] with the Gaussian 98 quantum chemistry software.[31]

Simulation of the dynamics: For the sake of simplicity, the molecule was modeled as pseudotriatomic with two collinear dissociative bonds q_a = [Re–H] and q_b = [Re–CO$_{ax}$] (Scheme 1). These two coordinates are the most significantly affected on going from the electronic ground state to the excited states and conserve the C_s symmetry. All other "spectator" modes

  0947-6539/02/0806-1362 $ 17.50+.50/0 *Chem. Eur. J.* **2002**, *8*, No. 6

are decoupled in this zero-order approximation. This decoupling mode should be reasonable, at least for the study of ultra-fast processes (below a few tens of ps).

The photo-absorption and the photo-dissociation dynamics are simulated by propagation of selected wavepackets $\psi_k(q_a, q_b, t)$ on the potentials $V^d_k(q_a, q_b)$ corresponding to the electronic states (k). The time evolution of the wavepacket is obtained by solving a set of coupled time-dependent Schrödinger equations in the diabatic representation given in Equation (3), with the initial conditions given in [Eq. (4)], where μ_k is the electronic transition dipole moment between the electronic ground state (gs) and the electronic excited state (k).

$$i\hbar\frac{\partial}{\partial t}\psi_k(q_a, q_b, t) = [T_{nu} + V^d_k]\psi_k(q_a, q_b, t) + \sum_{k\neq k'} V^d_{kk'}\psi(q_a, q_b, t) \quad (3)$$

$$\psi_k(q_a, q_b, t=0) = \mu_k \Phi_{gs,\,0,\,0}(q_a, q_b) \quad (4)$$

$\Phi_{gs,\,0,\,0}(q_a, q_b)$ represents the two-dimensional vibrational ground state wavefunction of the electronic ground state evaluated through the coupled Morse oscillators method.[32] In the case of preliminary one-dimensional simulations, along one of the coordinates q_a or q_b, the eigenstates of the electronic ground state are calculated through the Fourier Grid Hamiltonian method.[33]

The potential coupling $V^d_{kk'}$ is given either by the spin-orbit coupling elements of the SOC-CI matrix (singlet–triplet interactions) or by the transformation of the estimated kinetic couplings around avoided crossings (singlet–singlet and triplet–triplet interactions). The adiabatic/diabatic transformation is performed according to the scheme described in reference [27].

The solution of the time-dependent Schrödinger equation [Eq. (3)] is obtained by the Chebychev propagation scheme[34] with $\Delta t = 10$ fs. The propagations are based on representations either of $\Psi_k(q, t)$ on one-dimensional grids with the following parameters:

$q_{a_i} = q_{a_0} + (i-1)\Delta q_a; q_{a_0} = 2.65$ a.u., $\Delta q_a = 0.024$ a.u. with $1 \le i \le 512$

$q_{b_j} = q_{b_0} + (j-1)\Delta q_b; q_{b_0} = 3.118$ a.u., $\Delta q_b = 0.023$ a.u. with $1 \le j \le 512$

or of $\Psi_k(q_a, q_b, t)$ on two-dimensional grids with the following parameters:

$q_{a_i} = q_{a_0} + (i-1)\Delta q_a; q_{a_0} = 2.7$ a.u., $\Delta q_a = 0.187$ a.u. with $1 \le i \le 64$

$q_{b_j} = q_{b_0} + (j-1)\Delta q_b; q_{b_0} = 3.30$ a.u., $\Delta q_b = 0.022$ a.u. with $1 \le j \le 512$

The absorption spectrum σ_{tot} is obtained by the Fourier transform of the total autocorrelation function $S_{tot}(t)$ summed over the individual autocorrelation functions corresponding to each excited state k [Eq. (5)].

$$\sigma_{tot}(\omega) \propto \omega \int_{-\infty}^{+\infty} dt e^{i(E_i+\omega)t} S_{tot}(t) \quad (5)$$

Where $S_{tot}(t)$ is given by Equation (6) and E_i represents the energy of the initial wavepacket on the electronic state k.

$$S_{tot}(t) = \sum_k \langle \psi_k(0) \,|\, \psi_k(t) \rangle \quad (6)$$

The kinetic part of the Hamiltonian of the system, expressed in bond coordinates, is given by Equation (7), where μ_a and μ_b are the reduced masses corresponding to the bonds q_a and q_b, and m_c is the mass of the central atom.

$$T_{nu} = -\frac{\hbar^2}{2\mu_a}\frac{\partial^2}{\partial q_a^2} - \frac{\hbar^2}{2\mu_b}\frac{\partial^2}{\partial q_b^2} + \frac{\hbar^2}{m_c}\frac{\partial^2}{\partial q_a \partial q_b} \quad (7)$$

Reaction probabilities are deduced by integration, over the whole reaction time, of the probability current density expressed as a function of coordinates q_a and q_b [Eq. (8)],[35] where $J_a(q_a, q_b, t)$ is given in Equation (9) and $J_b(q_a, q_b, t)$ is defined in a symmetric way.

$$\vec{J}(q_a, q_b, t) = \begin{pmatrix} J_a(q_a, q_b, t) \\ J_b(q_a, q_b, t) \end{pmatrix} \quad (8)$$

$$J_a(q_a, q_b, t) = \frac{1}{\mu_a}\mathrm{Re}\left(\psi^*(q_a, q_b, t)\frac{\hbar\partial}{i\partial q_a}\psi(q_a, q_b, t)\right) + \frac{\cos\theta}{m_c}\mathrm{Re}\left(\psi^*(q_a, q_b, t)\frac{\hbar\partial}{i\partial q_b}\psi(q_a, q_b, t)\right) \quad (9)$$

In the case of preliminary one-dimensional simulations (along either q_a = [Re–H] or q_b = [Re–CO$_{ax}$] coordinates) the dissociation probability is simply given by Equation (10), where q_0 and q_{diss} represent the lower limit and the dissociation limit of the grid, respectively.

$$P_{diss}(t) = 1 - \sum_k \int_{q_0}^{q_{diss}} |\,\psi_k(q, t)\,|^2 dq \quad (10)$$

Results and Discussion

Geometrical structures: The geometrical structures were studied at the CASSCF level. Our purpose within the context of the present work was to infer the main qualitative trends when exciting the molecule. No further investigations of the dynamic correlation effects were taken into account in a post-CASSCF treatment. The agreement between the optimized bond lengths and bond angles and the experimental values is usually rather good for the electronic ground state, as shown in reference [17]. The CASSCF-optimized structure compares rather well with the DFT (B3LYP) structure for the a^{1}A′ electronic ground state, as illustrated by the values reported in parenthesis in Table 1. The largest deviation concerns the Re–CO$_{ax}$ bond length; however, it does not exceed 5 %. This difference may be attributed to the dynamic correlation effects included at the DFT level of theory (Re–CO$_{ax}$ 2.079 Å at the CASSCF level and 1.995 Å at the DFT level). Both values are in reasonable agreement with the experimental Re–CO$_{ax}$ bond lengths either in [Re(Me)(CO)$_3$(*i*Pr-dab)] (2.130 Å) or in [HRe(CO)$_5$] (2.00 Å).

To evaluate the structural deformations when going from the a^{1}A′ electronic ground state to the low-lying MLCT and SBLCT states, tentative geometry optimizations were per-

Table 1. Selected CASSCF-optimized bond lengths [Å] and bond angles [°] in the a^{1}A′ electronic ground state and low-lying ^{1,3}MLCT excited states.

	Experimental structure[a]	Idealized geometry	a^{1}A′ Electronic ground state[c]	b^{1}A′ $5d_{x^2-y^2} \rightarrow \pi^*_{H\text{-}dab}$	a^{3}A′ $5d_{xz} \rightarrow \pi^*_{H\text{-}dab}$
Re–H	(1.799)	1.799	1.746 (1.744, 1.737)	1.692	1.704
Re–C$_{ax}$	2.130	2.000	2.079 (1.969, 1.995)	2.174	2.277
Re–C$_{eq}$	1.910	2.000	1.980 (1.947, 1.962)	2.015	1.970
Re–N	2.177	2.177	2.116 (2.076, 2.102)	2.156	2.170
N-Re-C$_{eq}$	98.1	97.21	96.64 (93.98, 94.21)	98.29	94.45
Re-N-C	113.1	113.1	119.91 (119.5, 119.3)	116.43	116.40
H-Re-N	92.3 (90.5)[b]	83.7	91.7 (91.81, 91.72)	85.75	97.95
H-Re-C$_{eq}$	91.1 (86.3)[b]	83.7	79.68 (78.72, 78.78)	87.93	79.18
C$_{ax}$-Re-C$_{eq}$	86.9 (87.4)[b]	96.3	90.97 (82.45, 90.01)	97.61	91.86

[a] From the experimental structure of [HRe(CO)$_5$] for the Re–H bond length[19] and from [Re(Me)(CO)$_3$(*i*Pr-dab)] for the other bond lengths and bond angles.[18] [b] The values in parenthesis give the deviation of the bond angles with respect to the C_s symmetry of [Re(Me)(CO)$_3$(*i*Pr-dab)]. [c] The values in parenthesis correspond to the DFT (B3LYP) optimized structure with either the LANL2DZ library[29, 30] or the ECP Dolg library,[22, 23] respectively.

formed at the CASSCF level (8 e10 a) under the C_s symmetry constraint. The optimized structures of the lowest a^3A' MLCT state corresponding to the $3d_{xz} \rightarrow \pi^*_{H\text{-}dab}$ excitation and the b^1A' MLCT state corresponding to the $3d_{x^2-y^2} \rightarrow \pi^*_{H\text{-}dab}$ excitation, are reported in Table 1, together with the optimized geometry of the electronic ground state and the experimental bond lengths and bond angles of [Re(Me)-$(CO)_3$(*i*Pr-dab)]. Optimization of other electronic states failed because of convergence problems at the CASSCF level. In particular, it was not possible to optimise the structure of the molecule in the c^1A' MLCT state corresponding to the $3d_{xz} \rightarrow \pi^*_{H\text{-}dab}$ excitation which contributes mainly to the absorption spectrum and in the ^{3}SBLCT state that plays a key role in the photochemistry.

The main structural deformations of [Re(H)$(CO)_3$(H-dab)] after excitation to these low-lying states are represented in Figure 2. The flexibility of the molecule when going from the electronic ground state to the low-lying MLCT excited state is low. The small deformation of the model molecule in the MLCT states is in agreement with the presence of an intense emission at $\lambda = 500$ nm that matches perfectly with the absorption band and is typical of a number of MLCT complexes of this class investigated experimentally. The angular deformations never exceeded 10% and the only bond length elongation which exceeded 5% was the Re–CO_{ax} bond.

Most of the bond lengths are only slightly modified (<5%). It is worth noting that, whereas the Re–CO_{ax} bond length increases in the ^{1,3}MLCT states, the Re–H bond length decreases by about 3%. On the basis of these results, the theoretical study was restricted to the two coordinates q_a = [Re–H] and q_b = [Re–CO_{ax}], while the rest of the molecule was frozen into the ground state geometry. This is justified by the goal of the present work which deals with vertical transitions in the Franck–Condon domain followed by ultrafast dissociative processes occurring on the fs and ps time scales which are not competitive with vibrational relaxations.

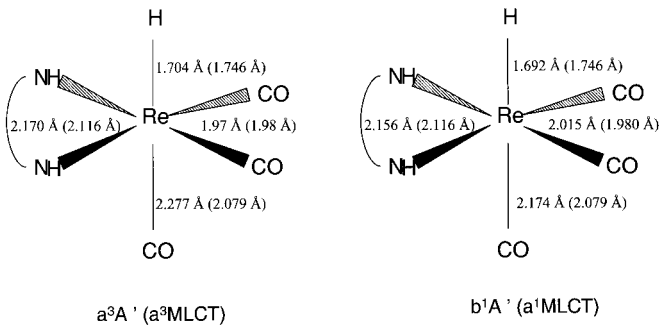

Figure 2. CASSCF-optimized geometries of the low-lying ^{1,3}MLCT excited states of [Re(H)$(CO)_3$(H-dab)] compared to the optimized geometry of the electronic ground state (values in parentheses). The bond lengths are given in Å.

Clearly, the study of other photophysical properties connected to long-lived excited states (e.g. emission spectra) should take account of the relaxation effects neglected in the present work.

Theoretical absorption spectrum: The CASSCF/MR-CCI transition energies to the low-lying singlet and triplet excited states of [Re(H)$(CO)_3$(H-dab)] are collected in Table 2. The multistate CASPT2 transition energies to the low-lying singlet A′ states are reported for comparison. As usual, the MR-CCI method overestimates the excitation energies by less than 2000 cm^{-1} (1520 cm^{-1} for the b^1A' MLCT state and 1900 cm^{-1} for the d^1A' SBLCT state). The large overestimation obtained for the second c^1A' MLCT state at the MR-CCI level must be pointed out. It can be explained by the mixed character of this state (with large contributions of the electronic ground state as well as of the low-lying MLCT and SBLCT states and others) characterized by a rather small main contribution in the CASSCF expansion (less than 60%). As a consequence, the quality of the zero-order CASSCF wavefunction is not equivalent for this state and the other states and the MR-CCI method hardly corrects this failure. Even though the MS-CASPT2 approach is better, this does not justify the use of this costly method for the computation of complicated 2D potential-energy surfaces with many avoided crossings where a perturbational approach that is not carefully driven may fail.

Table 2. CASSCF/MR-CCI transition energies [cm^{-1}] to the low-lying ^{1,3}A′ and ^{1,3}A″ excited states of [Re(H)$(CO)_3$(H-dab)] and corresponding oscillator strengths *f*. A few multi-state CASPT2 results are reported for comparison.

Transition	One-electron excitation in the principal configuration	CASSCF/MR-CCI	*f*	MS-CASPT2
$a^1A' \rightarrow a^3A'$	$5d_{xz} \rightarrow \pi^*_{H\text{-}dab}$	14330	–	
$a^1A' \rightarrow a^3A''$	$5d_{yz} \rightarrow \pi^*_{H\text{-}dab}$	15490	–	
$a^1A' \rightarrow c^1A''$	$5d_{yz} \rightarrow \pi^*_{H\text{-}dab}$	15800	≈0.0	
$a^1A' \rightarrow b^3A'$	$5d_{x^2-y^2} \rightarrow \pi^*_{H\text{-}dab}$	17310	–	
$a^1A' \rightarrow b^1A'$	$5d_{x^2-y^2} \rightarrow \pi^*_{H\text{-}dab}$	17440	≈0.0	15920
$a^1A' \rightarrow c^1A'$	$5d_{xz} \rightarrow \pi^*_{H\text{-}dab}$	22470	0.38	19390
$a^1A' \rightarrow d^3A'$	$\sigma_{Re\text{-}H} \rightarrow \pi^*_{H\text{-}dab}$	30420	–	
$a^1A' \rightarrow d^1A'$	$\sigma_{Re\text{-}H} \rightarrow \pi^*_{H\text{-}dab}$	33490	0.15	31590

The visible part of the absorption spectrum consists of three MLCT states corresponding to $3d \rightarrow \pi^*_{H\text{-}dab}$ excitations and ranging between 15490 and 22470 cm^{-1}. The c^1A' ($3d_{xz} \rightarrow \pi^*_{H\text{-}dab}$) state is the only one which has a large enough oscillator strength ($f = 0.38$) to contribute significantly to the visible absorption. The UV absorption is composed of the SBLCT state (d^1A') corresponding to the $\sigma_{Re\text{-}H} \rightarrow \pi^*_{H\text{-}dab}$ excitation calculated at 33490 cm^{-1} with an oscillator strength of 0.15. The calculation of the triplet states was restricted to the few states which may participate in the early photochemistry, namely the low-lying MLCT states (a^3A', a^3A'', b^3A') and the ^{3}SBLCT (c^3A') state which is dissociative for the Mn–H bond. The singlet–triplet energy gap (<3000 cm^{-1}) is small for the excited states delocalized on the $\pi^*_{H\text{-}dab}$ acceptor ligand (MLCT or SBLCT). The particular behavior of the MLCT state corresponding to the $3d_{xz} \rightarrow \pi^*_{H\text{-}dab}$ is caused by an important interaction between its singlet component with the electronic ground state. This interaction explains the

  0947-6539/02/0806-1364 $ 17.50+.50/0 *Chem. Eur. J.* **2002**, *8*, No. 6

unusually large singlet–triplet energy gap ($\approx$1.0 eV) for this MLCT state, which is a consequence of the singlet component destabilization. The character of the low-lying triplet excited states of [Re(H)(CO)$_3$(H-dab)] in the Franck–Condon region is rather pure, either MLCT or SBLCT. The composition of the singlet MLCT state corresponding to the $3d_{xz} \rightarrow \pi^*_{H\text{-}dab}$ excitation points to a significant mixing with the ^{1}SBLCT state and vice versa, which was not observed in the manganese complex.[17]

The main effect of the metal center is a lowering of the MLCT and SBLCT excited states on going from the manganese to the rhenium complex. This is mainly caused by the stabilization of the $\pi^*_{H\text{-}dab}$ orbital by interaction with the diffuse $6p_z$ orbital of the third row transition metal atom. The relativistic destabilization of the 5d orbitals also contributes to the lowering of the MLCT states.

The SOC terms between the low-lying triplet and singlet states and the SO splitting of the triplet states are reported in Table 3. SOC values were evaluated through a restricted full-CI scheme[36] based on a unique CASSCF wavefunction optimized either for the triplet states or for the singlet states. The SO splitting of the triplet states obtained after diagonalization of the SOC-CI matrix never exceeds 1230 cm^{-1} (vs. 60 cm^{-1} for [Mn(H)(CO)$_3$(H-dab)][36]), value obtained for the ^{3}MLCT state calculated at 17310 cm^{-1} and corresponding to the $5d_{x^2-y^2} \rightarrow \pi^*_{H\text{-}dab}$ excitation. This significant SO splitting should not allow direct absorption to this triplet state. Indeed, although it is very close to the corresponding ^{1}MLCT state calculated at 17440 cm^{-1}, the negligible oscillator strength ($f \approx 0.0$) of this latter state makes the absorption ineffective. The SO splitting of the other triplet states ranges between 80 and 310 cm^{-1} and should not significantly affect the absorption spectrum. However, one has to keep in mind the possibility of a fast indirect population of the low-lying triplet states after vertical absorption to the ^{1}MLCT state corresponding to the $3d_{xz} \rightarrow \pi^*_{H\text{-}dab}$ excitation, which leads to a small perturbation of the absorption spectrum (see the next section). The SOC values range between 100 and 560 cm^{-1} (vs. 0–100 cm^{-1} in the manganese complex).

The theoretical spectrum (Figure 3a) was obtained by propagation of the $\psi_{b^1A'}(q_a, q_b, t)$, $\psi_{c^1A'}(q_a, q_b, t)$ and $\psi_{d^1A'}(q_a, q_b, t)$ wavepackets on the corresponding b^1A', c^1A' and d^1A' PES [Eqs. (11–13)] (the details of the simulation are described in the next sections) with the initial conditions given by Equation (4).

$$\psi_{b^1A'}(q_a, q_b, t=0) = 0.0377\, \Phi_{a^1A'0,0}(q_a, q_b) \quad (11)$$

$$\psi_{c^1A'}(q_a, q_b, t=0) = 0.8817\, \Phi_{a^1A'0,0}(q_a, q_b) \quad (12)$$

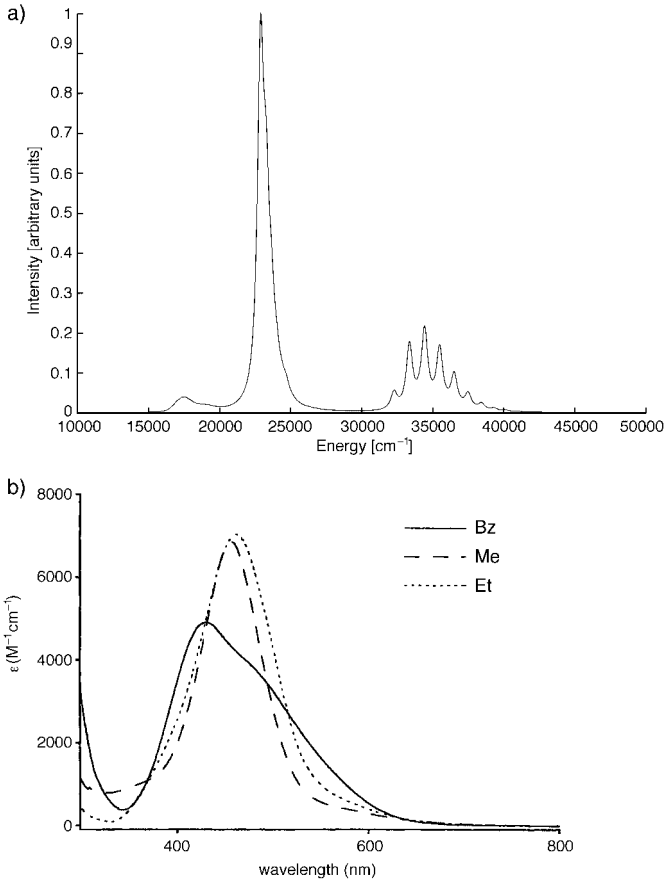

Figure 3. a) Theoretical absorption spectrum of [Re(H)(CO)$_3$(H-dab)] (the envelope was obtained after multiplication of the original autocorrelation function by an exponential factor exp ($-\Gamma t$), $\Gamma = 0.13$). b) Experimental absorption spectrum of [Re(R)(CO)$_3$(*i*Pr-dab)] measured in THF at room temperature.

$$\psi_{d^1A'}(q_a, q_b, t=0) = 0.4704\, \Phi_{a^1A'0,0}(q_a, q_b) \quad (13)$$

The theoretical absorption spectrum (Figure 3a) exhibits an intense peak centered around 23000 cm^{-1} (430 nm), in agreement with the experimental spectrum recorded for [Re(R)(CO)$_3$(*i*Pr-dab)] (R = Me, Et) between 300 and 700 nm (Figure 3b). A shoulder at $\approx$35000 cm^{-1} (285 nm) and a weak absorption at 15000 cm^{-1} (666 nm), beyond the experimental detection limits, are also present in the theoretical spectrum. The intense band and the weak absorption in the visible energy domain can be attributed to the $a^1A' \rightarrow c^1A'$ and $a^1A' \rightarrow b^1A'$ MLCT transitions, respectively, whereas the UV absorption corresponds to the $a^1A' \rightarrow d^1A'$ SBLCT transition.

Table 3. Calculated spin-orbit interactions [cm^{-1}] in [Re(H)(CO)$_3$(H-dab)] at the CASSCF/SOC-CI level (Z_{eff} = 60.0). This work and ref. [36].

	a^3A' $5d_{xz} \rightarrow \pi^*_{H\text{-}dab}$ MLCT	b^3A' $5d_{x^2-y^2} \rightarrow \pi^*_{H\text{-}dab}$ MLCT	d^3A' $\sigma_{Re-H} \rightarrow \pi^*_{H\text{-}dab}$ SBLCT
a^1A' electronic ground state	190	370	370
b^1A' $5d_{x^2-y^2} \rightarrow \pi^*_{H\text{-}dab}$ MLCT	560	160	230
c^1A' $5d_{xz} \rightarrow \pi^*_{H\text{-}dab}$ MLCT	130	530	310
d^1A' $\sigma_{Re-H} \rightarrow \pi^*_{H\text{-}dab}$ SBLCT	390	150	100

Potential energy curves for the homolytic rupture of the rhenium–hydrogen bond: Table 4 gives the MR-CCI energies for the a^1A' electronic ground state and the low-lying singlet and triplet excited states of [Re(H)(CO)$_3$(H-dab)] of A′ symmetry, calculated along the Re–H bond homolysis reaction

Table 4. MR-CCI energies values (in au and relative to – 174) of the electronic ground state (a^1A') and low-lying excited states of [Re(H)$(CO)_3$(H-dab)] as a function of q_a = [Re–H] (Re–CO_{ax} 2.00 Å).

	Re–H									
	1.5 Å	1.6 Å	1.799 Å	1.9 Å	2.0 Å	2.2 Å	2.5 Å	2.9 Å	3.5 Å	50.0 Å
a^1A'	0.60567	0.62042	0.628930	0.62515	0.61899	0.60469	0.58274	0.55408	0.53887	0.53253
b^1A'	0.54046	0.55226	0.55128	0.54722	0.54156	0.52683	0.50208	0.48794	0.47832	0.47283
c^1A'	0.50902	0.52283	0.52723	0.52378	0.51833	0.50422	0.49086	0.48407	0.47034	0.46853
d^1A'	0.43130	0.45477	0.47577	0.48088	0.48405	0.48702	0.47708	0.45811	0.44245	0.42815
a^3A'	0.55182	0.56372	0.56552	0.56201	0.55576	0.54254	0.53337	0.53162	0.53366	0.53480
b^3A'	0.54093	0.55196	0.55068	0.54722	0.54181	0.52780	0.50590	0.48391	0.47538	0.47499
c^3A'	0.44405	0.46853	0.49260	0.49546	0.50335	0.50976	0.50199	0.48390	0.47293	0.47213

path under the C_s symmetry constraint. The corresponding adiabatic and diabatic potential-energy curves are shown in Figure 4a and 4b, respectively.

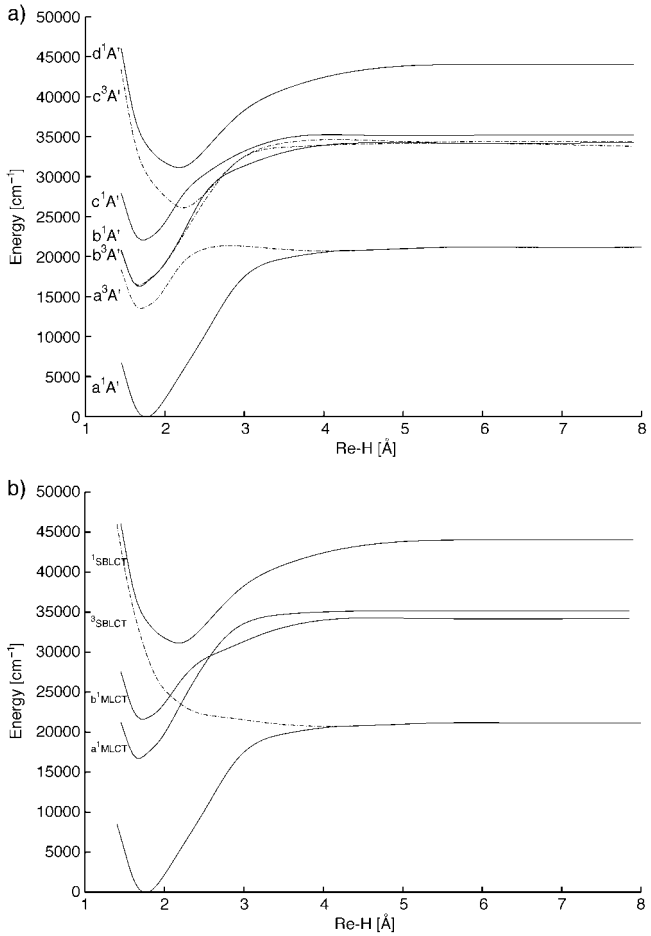

Figure 4. a) CASSCF/MR-CCI Potential energy curves (PEC) along the q_a = [Re–H] bond elongation in [Re(H)$(CO)_3$(H-dab)] for the low-lying singlet (solid lines) and triplet (dashed lines) excited states. b) Diabatic PEC obtained by transformation of the previous one for the a^1A' electronic ground state, the b^1MLCT absorbing state and the ^{3}SBLCT state.

The reaction is calculated to be endothermic by 60.5 kcal mol^{-1}, in agreement with the Re–H bond energy in transition metal hydrides.[37] The formation of the diradical H$^{\cdot}$ + [$^{\cdot}$Re-$(CO)_3$(H-dab)] primary products rests on the change of character of the a^1A' potential as a function of q_a = [Re–H]. At the equilibrium (q_a = 1.799 Å), a^1A' is described by the following electronic configuration $(\sigma_{Re-H})^2(5d_{x^2-y^2})^2(5d_{yz})^2$-$(5d_{xz})^2(\sigma^*_{Re-H})^0$, where the σ_{Re-H} and σ^*_{Re-H} orbitals are bonding and antibonding combinations of the s_H orbitals with the $5d_{z^2} + \varepsilon\pi^*_{H\text{-}dab}$ and $5d_{z^2} - \varepsilon\pi^*_{H\text{-}dab}$, respectively. The $\pi^*_{H\text{-}dab}$ character of these latter orbitals increase as a function of the q_a coordinate leading to $\pi^*_{H\text{-}dab} + 5d_{z^2}$ and $5d_{z^2} - \pi^*_{H\text{-}dab}$ combinations at the asymptot. At dissociation, the electronic configuration of the a^1A' state is given by $(s_H)^2(5d_{x^2-y^2})^2$-$(5d_{yz})^2(5d_{xz})^2(\pi^*_{H\text{-}dab} + 5d_{z^2})^0 - (s_H)^0(5d_{x^2-y^2})^2(5d_{yz})^2(5d_{xz})^2$-$(\pi^*_{H\text{-}dab} + 5d_{z^2})^2$ which is nearly degenerate (see Table 4) with the corresponding a^3A' $(s_H)^1(5d_{x^2-y^2})^2(5d_{yz})^2(5d_{xz})^2(\pi^*_{H\text{-}dab} + 5d_{z^2})^1$ describing the formation of the di-radicals. The low-lying MLCT states, namely b^1A' and c^1A', are bound and they generate an avoided crossing at ≈2.6 Å. The singlet states are bound along the q_a coordinate and should not lead to fast direct homolytic cleavage of the Re–H bond after visible absorption into the MLCT states.

The shape of the triplet potentials (Figure 4a) indicates the presence of two low-lying bound states, namely the a^3A' and b^3A' MLCT states. The c^3A' state corresponding to the $\sigma_{Re-H} \rightarrow \pi^*_{H\text{-}dab}$ excitation is dissociative and generates several avoided crossings at 2.20 Å and 2.27 Å with the b^3A' and a^3A' states, respectively. Consequently, the a^3A' state is predissociative with a small energy barrier (< 5.0 kcal mol^{-1} compared to the energy barrier of 21.0 kcal mol^{-1} for the manganese complex) along the reaction pathway. The shape of the potential energy curve along the metal – hydrogen bond elongation is very similar in both complexes ([Mn(H)-$(CO)_3$(H-dab)] and [Re(H)$(CO)_3$(H-dab)]). The main differences which may influence the photo-reactivity are the small energy barrier on the predissociative a^3A' state and the occurrence of a crossing between the singlet absorbing state (c^1A' MLCT) and the triplet dissociative state (c^3A' SBLCT) earlier in the reaction path in the case of the rhenium complex. This crossing point appears clearly on the diabatic potentials shown in Figure 4b.

Potential energy curves for the axial carbonyl loss: Table 5 gives the MR-CCI energies for the a^1A' electronic ground state and the low-lying singlet and triplet excited states of [Re(H)$(CO)_3$(H-dab)] of A′ symmetry, calculated along the Mn–CO_{ax} bond dissociation pathway under the C_s symmetry constraint.

The corresponding adiabatic potential-energy curves which coincide with the diabatic curves in this case (no avoided crossing situations similar to those found along the Re–H bond homolysis reaction path) are shown in Figure 5. The

  0947-6539/02/0806-1366 $ 17.50+.50/0 *Chem. Eur. J.* **2002**, *8*, No. 6

Table 5. MR-CCI energies values (in au and relative to – 174) of the electronic ground state (a^1A') and low-lying excited states of [Re(H)(CO)$_3$(H-dab)] as a function of q_b = [Re–CO$_{ax}$] (Re–H 1.799 Å).

	Re–CO$_{ax}$									
	1.7 Å	1.9 Å	2.0 Å	2.1 Å	2.2 Å	2.4 Å	2.7 Å	2.9 Å	4.0 Å	50.0 Å
a^1A'	0.57357	0.62360	0.62893	0.62732	0.62239	0.60944	0.59354	0.58655	0.57612	0.57218
b^1A'	0.48990	0.54292	0.55128	0.55447	0.55386	0.54741	0.53886	0.53534	0.53170	0.52953
c^1A'	0.45933	0.51792	0.52723	0.52926	0.52719	0.51652	0.50266	0.49689	0.49216	0.49416
d^1A'	0.43050	0.47352	0.47577	0.47264	0.46696	0.45288	0.43567	–	–	0.42284
a^3A'	0.49102	0.55398	0.56552	0.56935	0.57087	0.56736	0.55989	0.55706	0.55396	0.54921
b^3A'	0.48665	0.54158	0.55068	0.55245	0.55440	0.54784	0.53799	0.53431	0.53188	0.52736
c^3A'	0.45094	0.49187	0.49260	0.48833	0.48115	0.46579	0.44876	–	–	0.42293

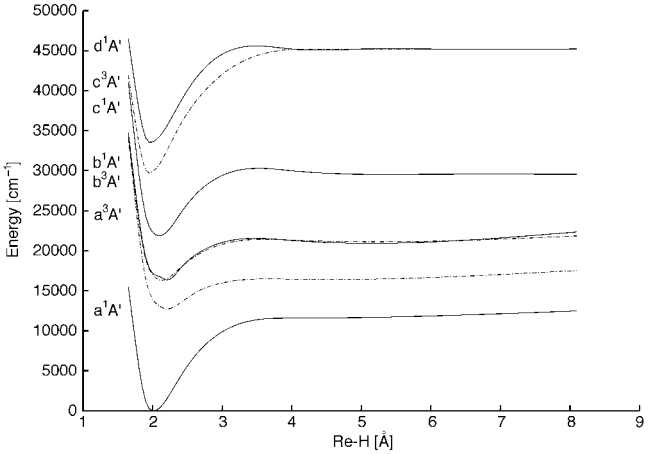

Figure 5. CASSCF/MR-CCI Potential energy curves (PEC) along the q_b = [Re–CO$_{ax}$] bond elongation in [Re(H)(CO)$_3$(H-dab)] for the low-lying singlet (solid lines) and triplet (dashed lines) excited states.

reaction is calculated to be endothermic by 35.6 kcal mol^{-1}. This value is in the range of the experimental data available for the metal–carbonyl bond dissociation energy in transition metal carbonyls.[38]

In contrast to the manganese analogue [Mn(H)(CO)$_3$-(H-dab)], the low-lying singlet and triplet MLCT states (b^1A', c^1A', a^3A' and b^3A') are bound along this reaction path. The bound character of the MLCT states in [Re(H)(CO)$_3$(H-dab)] is mainly caused by different electronic interactions in the two analogues. In particular, a very weak dπ–pπ back-bonding interaction between the Re atom and the axial CO ligand (compensated by a σ interaction with the diffuse 6p orbital of Re) which contrasts to the strong one occurring between the Mn atom and the axial CO ligand (Scheme 2), prevents a significant weakening of the Re–CO$_{ax}$ bond when an electron is excited from the 5d orbitals of the metal into the $\pi^*_{H\text{-}dab}$ orbital. This is illustrated by the increase of the M–CO$_{ax}$ bond lengths in both complexes when going from the electronic ground state to the ^{1,3}MLCT states. In the manganese complex, this change ranges between 6% (^{1}MLCT) to 14% (^{3}MLCT), whereas in the rhenium complex it never exceeds 9%. The triplet and singlet components of the SBLCT (d^1A' and c^3A') are bound

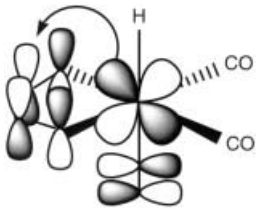

Scheme 2.

for this reaction pathway; in particular for the c^3A' state corresponding to the $\sigma_{Re-H} \rightarrow \pi^*_{H\text{-}dab}$ excitation, which is dissociative for the concurrent reaction, namely Re–H bond homolysis.

The two-dimensional diabatic potential energy surfaces (PES) obtained by transformation of the adiabatic PES calculated with CASSCF/MR-CCI as a function of q_a = [Re–H] and q_b = [Re–CO$_{ax}$] reaction coordinates under the C_s symmetry constraint (see Scheme 1) are represented in Figure 6a and 6b for the c^1A' MLCT and c^3A' SBLCT states, respectively. These 2D PES were interpolated by means of the bicubic spline scheme on the basis of 40 to 50 ab initio points. As illustrated by the shape of the c^1A' PES, the b^1MLCT state, which absorbs in the visible, is bound in both directions of dissociation (axial CO loss and Re–H bond homolysis). Within the limit of this 2D representation, the only possible reactive deactivation channel goes through the dissociative valley of the c^3A' PES (Figure 6b) along the Re–H bond homolysis via the b^1MLCT $\rightarrow$ ^{3}SBLCT intersystem crossing. On the basis of the calculated excited states and associated PES, the following qualitative mechanism is proposed:

After the $a^1A' \rightarrow c^1A'$ transition, which populates the b^1MLCT state, the system becomes trapped in its potential well. The only possibility of fast deactivation (on the ps timescale) of the excited molecule within the limit of the 2D model is an indirect Re–H bond homolysis via $c^1A' \rightarrow c^3A'$ intersystem crossing at ≈2.1 Å (see Figure 4b) leading to the radical H$^\cdot$ + $^\cdot$[Re(CO)$_3$(H-dab)] primary products in their ^{1,3}A′ ground state.

To obtain a quantitative mechanism with information on the time scales and probabilities of the primary reactions, on the population of the different excited states after visible irradiation and on the efficiency of intersystem crossing processes, several 1D and 2D simulations of the excited-state dynamics were performed with wavepacket propagations on spin-orbit and non-adiabatically coupled potentials.

One-dimensional simulation on spin-orbit coupled potentials: To select the excited states that play a key role in the photodissociation mechanism and to determine the contribution of the triplet states, one-dimensional wavepacket propagations either along the q_a = [Re–H] reaction coordinate or along the q_b = [Re–CO$_{ax}$] reaction coordinate were performed on spin-orbit and non-adiabatically coupled potentials. Six potentials were included in the simulation of the

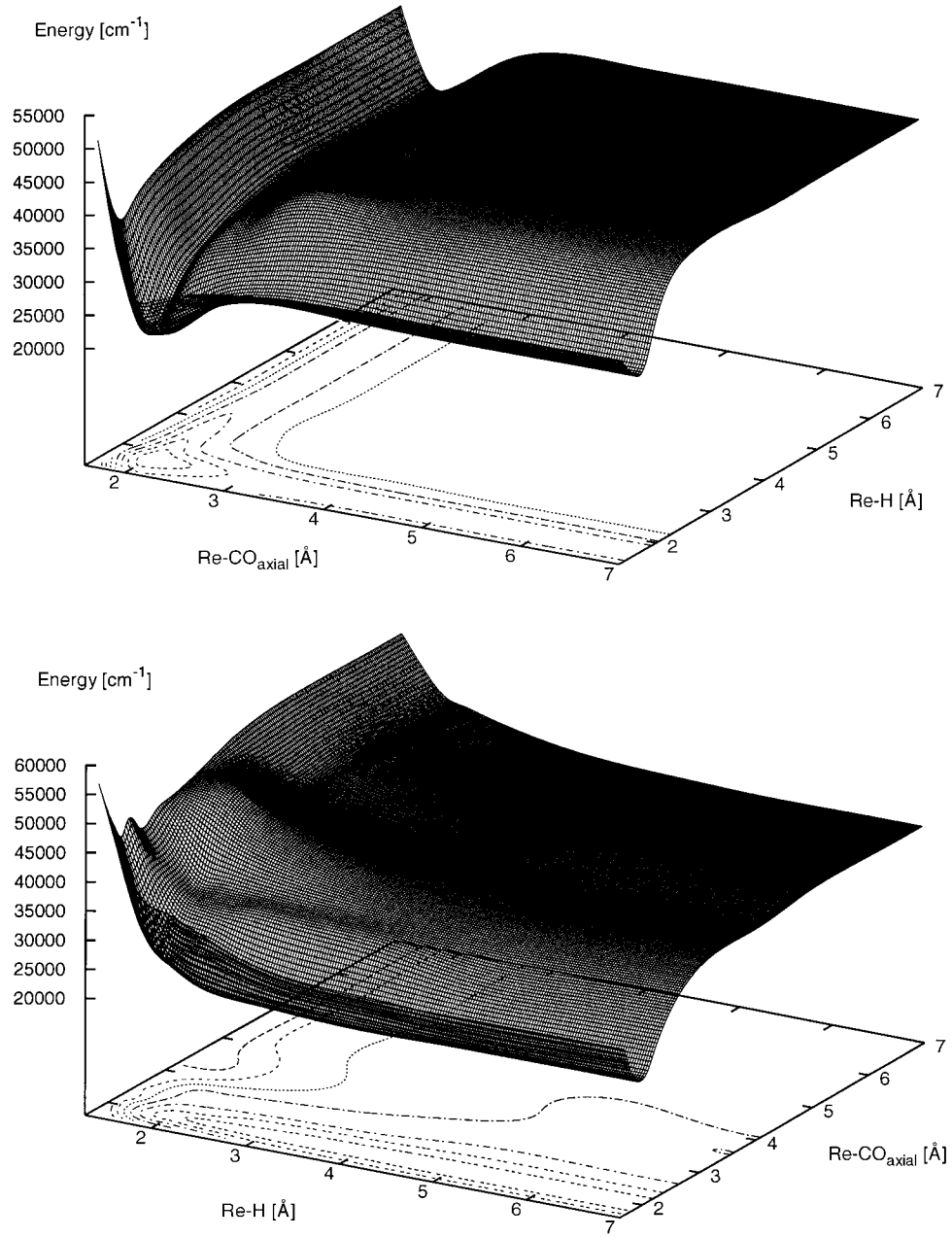

Figure 6. Two-dimensional diabatic potential energy surfaces (PES) as a function of the $q_a = [Re{-}H]$ and $q_b = [Re{-}CO_{ax}]$ bond elongations for a) the b^1MLCT absorbing state and b) the ^{3}SBLCT excited state of $[Re(H)(CO)_3(H\text{-}dab)]$.

dynamics after absorption in the visible: the a^1A' electronic ground state, the b^1A', c^1A' MLCT states ranging in the absorption energy domain and the three triplet states corresponding to the a^3A', b^3A' MLCT states and c^3A' (SBLCT) states.

The initial conditions used for the simulation of the visible absorption to the low-lying MLCT states are given in Equations (14) and (15).

$$\psi_{b^1A'}(q, t=0) = 0.0377\,\Phi_{a^1A'0}(q) \quad (14)$$

$$\psi_{c^1A'}(q, t=0) = 0.8817\,\Phi_{a^1A'0}(q) \quad (15)$$

Investigation of the population of the different excited states after 1 ps of simulation of the reaction path of Re–H bond homolysis (Figure 7) points to an important exchange between the two ^{1}MLCT bound states. At $t = 0$, 95% of the system stands is in the c^1A' state. In the first tens of fs, the population of the b^1A' state increases to 30%. The perfect correlation between the population of the b^1A' state and the depopulation of the c^1A' state with an oscillating behavior characterized by a period of 28 fs (Figure 7a, b). After 1 ps of simulation no significant damping is observed. The singlet–triplet intersystem crossing processes are inefficient on this time scale according to the low population of the low-lying triplet states after 1 ps. The only significant population concerns the b^3MLCT, which reaches 15% and can be attributed to two features: 1) the large spin-orbit interaction between this state and the b^1MLCT absorbing state (530 cm^{-1}); 2) the near-degeneracy of this triplet state with

  0947-6539/02/0806-1368 $ 17.50+.50/0 *Chem. Eur. J.* **2002**, *8*, No. 6

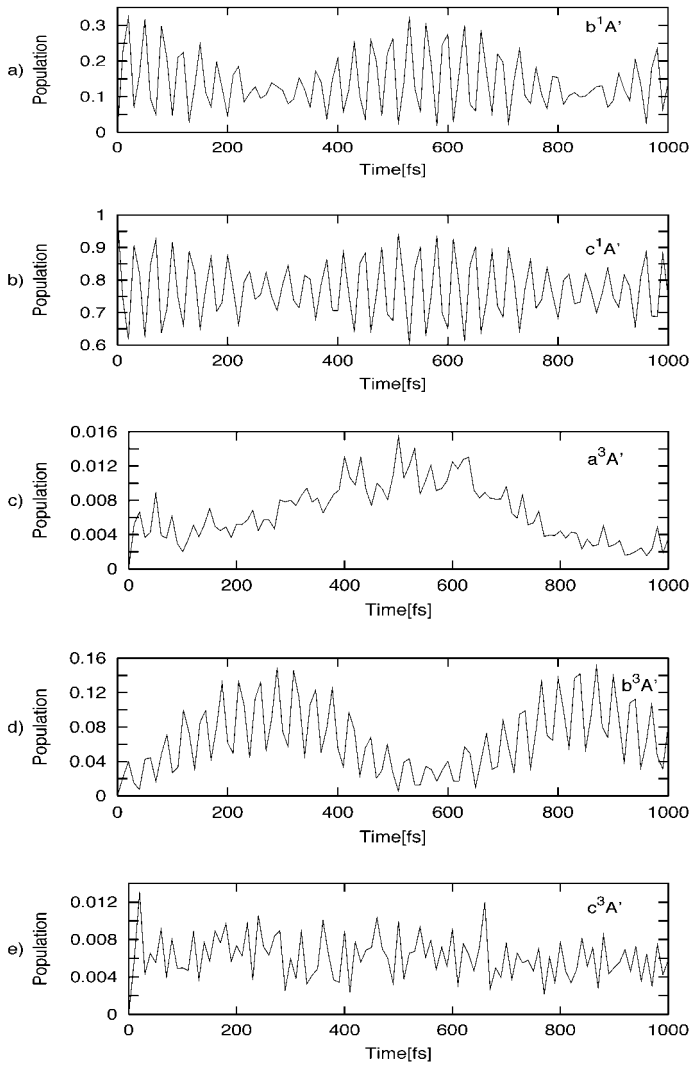

Figure 7. Evolution of the low-lying excited states population of [Re(H)-(CO)$_3$(H-dab)] after irradiation in the visible as a function of time (along the q_a = [Re–H] bond coordinate).

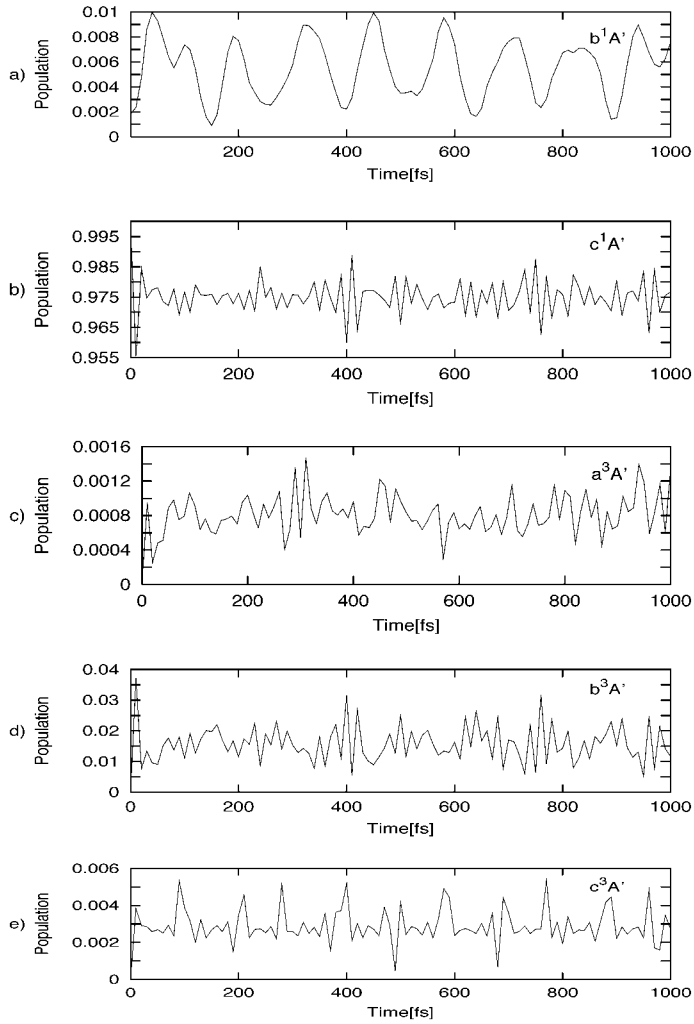

Figure 8. Evolution of the population of the low-lying excited states of [Re(H)(CO)$_3$(H-dab)] after irradiation in the visible as a function of time (along the q_b = [Re–CO$_{ax}$] coordinate).

the a^{1}MLCT state in the Franck – Condon region. The second factor is illustrated by the correlation between the population evolution of these two states as a function of time (Figure 7a, d) which follows an oscillating behavior with a period of ≈600 fs. Surprisingly, the population of the ^{3}SBLCT state dissociative for the Re–H bond homolysis is very small, despite the presence of a crossing between this state and the b^{1}MLCT absorbing state at ≈2.15 Å (Figure 4b). Within this 1D picture, as soon the wavepacket reaches the ^{1}MLCT state it gets trapped in its potential well and starts an oscillating motion. It looses energy by relaxation to the a^{1}MLCT and b^{3}MLCT states prior to reaching this crossing point.

The populations of the different excited states after 1 ps of simulation along the Re–CO$_{ax}$ bond reaction coordinate are reported in Figure 8. The b^{1}MLCT absorbing state remains mainly populated (>95%) and there is no significant exchange with the other states (either singlet or triplet) along this reaction pathway.

On the basis of these results, only the b^{1}MLCT absorbing state (c^{1}A′) and ^{3}SBLCT (c^{3}A′) dissociative state for the Re–H bond homolysis were retained in the 2D simulation. Although the a^{1}MLCT state is significantly populated by exchange with the b^{1}MLCT absorbing state, it was not included in the 2D simulation because, according to its bound character, it should not participate in the photo-reactivity of [Re(R)(CO)$_3$(H-dab)].

Two-dimensional simulation of the photodissociation dynamics after absorption in the visible region: The time evolution of the system was followed by propagation of the $\psi_{c^1A'}(q_a, q_b, t)$ and $\psi_{c^3A'}(q_a, q_b, t)$ wavepackets on the $V_{c^1A'}(q_a, q_b)$ and $V_{c^3A'}(q_a, q_b)$ potentials coupled non-adiabatically and by spin-orbit with the initial conditions given in Equations (16–18).

$$\psi_{b^1A'}(q_a, q_b, t=0) = 0 \quad (16)$$

$$\psi_{c^3A'}(q_a, q_b, t=0) = 0 \quad (17)$$

$$\psi_{c^1A'}(q_a, q_b, t=0) = 1.0\,\Phi_{a^1A',0,0}(q_a, q_b) \quad (18)$$

After the initial a^{1}A′ → c^{1}A′ transition, the wavepacket gets trapped in the potential well of the b^{1}MLCT absorbing state,

as depicted in Figure 9. On a very short time scale (50 fs), the c^3A' (^{3}SBLCT) state is populated. As soon as the wavepacket reaches this potential it evolves along the dissociative channel towards the formation of the diradical $H^{\bullet} + {}^{\bullet}[Re(CO)_3(H\text{-dab})]$ primary products in their $^{1,3}A'$ ground state. This

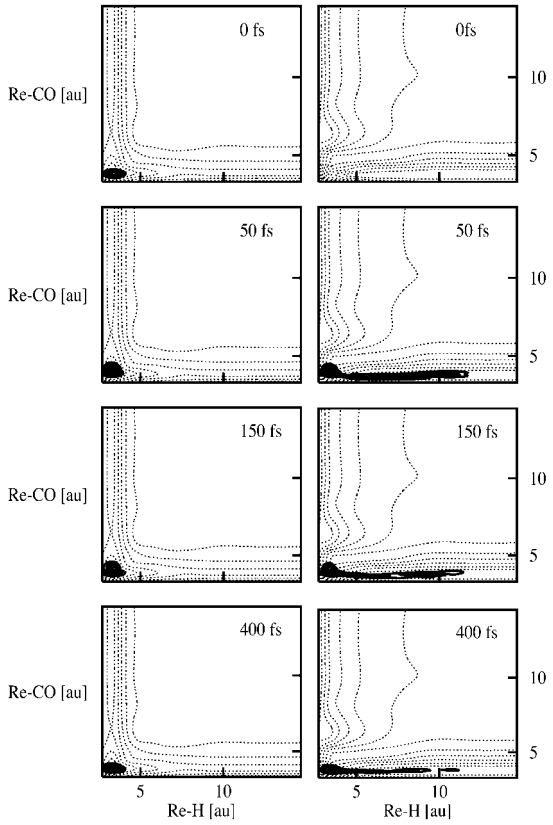

Figure 9. Time evolution of the $\psi_{c^1A'}(q_a, q_b, t)$ wavepacket (solid line) on the $V_{c^1A'}(q_a, q_b)$ potential (dashed line) (left) and of the $\psi_{c^3A'}(q_a, q_b, t)$ wavepacket (solid line) on the $V_{c^3A'}(q_a, q_b)$ potential (dashed line) (right).

indirect homolysis of the Re–H bond in $[(H)Re(CO)_3(H\text{-dab})]$ via $b^1MLCT \rightarrow {}^3SBLCT$ intersystem crossing is rather slow and inefficient in the first ps, as illustrated by the dissociation probability reported in Figure 10, which remains lower than 2% after 3 ps of simulation.

This result is in perfect agreement with the quantum yield (0.01–0.12) of the Re–Me bond observed in the dab-substituted methyl complexes $[Re(Me)(CO)_3(i\text{Pr-dab})]$.[4–6]

Conclusion

The electronic spectroscopy and photo-dissociation dynamics of $[Re(H)(CO)_3(H\text{-dab})]$, a model system for a series of $[M(R)(CO)_3(\alpha\text{-diimine})]$ complexes of great importance in catalytic, polymerization or electron/energy transfer chemistry induced by light, were investigated by means of wavepacket propagations on ab initio potentials calculated for the electronic ground and low-lying MLCT and SBLCT excited states. The effect of the metal center on the photoreactivity of this class of $[M(R)(CO)_3(\alpha\text{-diimine})]$ complexes on going from the first-row transition metal (Mn) to the third-row (Re)

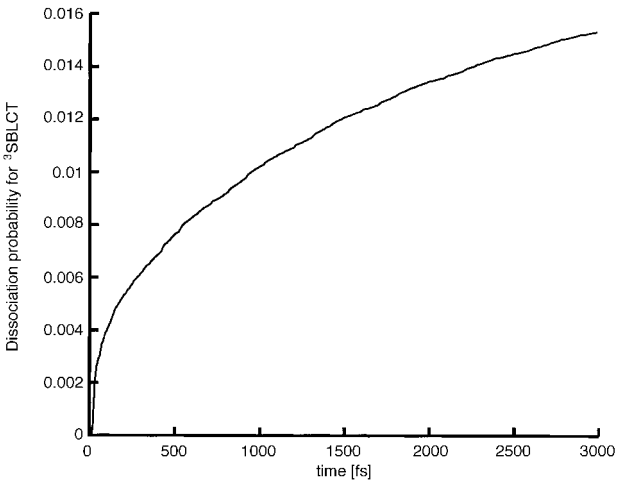

Figure 10. Probability of the indirect Re–H bond homolysis in $[Re(H)(CO)_3(H\text{-dab})]$ as a function of time after irradiation in the visible.

was the main motivation of this work accomplished in the context of a broad field of theoretical/experimental research on metal-to-ligand charge-transfer complexes carried out over a period of many years.

In contrast to the manganese complex $[Mn(H)(CO)_3(H\text{-dab})]$,[17] only one reactive channel of deactivation is accessible after irradiation in the visible energy domain, namely homolysis of the metal–hydrogen bond leading to $H^{\bullet} + {}^{\bullet}[Re(CO)_3(H\text{-dab})]$. Within the limit of the 2D simulation performed on the ps time scale, the photoreactivity is characterized by a rather inefficient indirect dissociation via the $b^1MLCT \rightarrow {}^3SBLCT$ intersystem crossing. Moreover, the probability of dissociation remains very low (<2%) after 3 ps of simulation. This points to a non-total process as compared to the direct, total and ultrafast CO loss (<500 fs) observed in $[Mn(H)(CO)_3(H\text{-dab})]$. This result is in agreement with the modest quantum yield characterizing the Re–Me bond homolysis in the methyl-substituted Re complexes.

The photodissociation dynamics is controlled by the $b^1MLCT/{}^3SBLCT$ spin-orbit coupling and the position of their crossing along the reactive channel. The proposed mechanism explains the wavelength and temperature dependence of the quantum yield in $[M(R)(CO)_3(\alpha\text{-diimine})]$ (R = methyl).[6] Indeed, by increasing the wavelength of the irradiation or the temperature, the system will gain some vibrational energy in the b^1MLCT absorbing state. Consequently, by a simple dynamic effect, the probability of reaching the $b^1MLCT/{}^3SBLCT$ crossing point (which is well above the b^1MLCT minimum) will increase as well.

In agreement with experimental observations, CO loss is quenched in the rhenium complexes due to the bound character of the PES along this pathway. Indeed, the very weak $d\pi - p\pi$ back-bonding interaction between the Re atom and the axial CO ligand observed in the model system $[Re(H)(CO)_3(H\text{-dab})]$ prevents a significant weakening of the $Re{-}CO_{ax}$ bond when exciting the molecule into the ^1MLCT state. The only deactivation channel concurrent to the Re–H bond homolysis is the $b^1MLCT \rightarrow b^3MLCT$ transition leading to an unreactive state with a long lifetime (ns time scale). This branching of the evolution of the Franck–Condon excited

0947-6539/02/0806-1370 $ 17.50+.50/0 *Chem. Eur. J.* **2002**, *8*, No. 6

state between trapping and reactive states has been observed recently for the similar [Re(Me)(CO)$_3$(dmb)] complex.[9] The branching time of less than 400 fs, determined by femtosecond time-resolved absorption spectroscopy, is in agreement with the simulation of the b^{1}MLCT absorbing state dynamics which shows that more than 95 % of the system still gets trapped in the b^{1}MLCT potential well after 500 fs of propagation.

The effect of the radical R on the photoreactivity of the [M(R)(CO)$_3$(α-diimine)] complexes (R = Me, Et, Bz; and M = Mn, Re) which has been extensively studied experimentally, was investigated for two model complexes [M(Et)(CO)$_3$(H-dab)] (M = Mn, Re) and will be the subject of a further article.[39] The solvent effects which are not taken into account here are beyond the scope of the present investigation of the early excited states dynamics based on accurate quantum chemical calculations. However, they should be investigated in the near future.

Acknowledgement

This work was undertaken as a part of the European Collaborative COST project (D14/0001/99). We thank the Departement de Chimie of the CNRS for the specific COST financial support. The quantum chemical calculations were carried out either at the IDRIS (Orsay, France) through a grant of computer time from the Conseil Scientifique, or at the LCQS (Strasbourg, France).

[1] D. J. Stufkens, *Comments Inorg. Chem.* **1992**, *13*, 359.
[2] D. J. Stufkens, A. Vlček, Jr, *Coord. Chem. Rev.* **1998**, *177*, 127.
[3] D. J. Stufkens, M. P. Aarnts, J. Nijhoff, B. D. Rossenaar, A. Vlček, Jr, *Coord. Chem. Rev.* **1998**, *171*, 93.
[4] D. J. Stufkens, J. M. W. van Outerstep, A. Oskam, B. D. Rossenaar, G. J. Stor, *Coord. Chem. Rev.* **1994**, *132*, 147; B. D. Rossenaar, C. J. Kleverlaan, D. J. Stufkens, A. Oskam, *J. Chem. Soc. Chem. Commun.* **1994**, 63.
[5] B. D. Rossenaar, D. J. Stufkens, A. Oskam, J. Fraanje, K. Goubitz, *Inorg. Chim. Acta* **1996**, *247*, 215.
[6] B. D. Rossenaar, C. J. Kleverlaan, M. C. E. van de Ven, D. J. Stufkens, A. Vlček, Jr, *Chem. Eur. J.* **1996**, *2*, 228.
[7] L. A. Lucia, R. D. Burton, K. S. Schanze, *Inorg. Chim. Acta* **1993**, *208*, 103.
[8] C. J. Kleverlaan, D. M. Martino, H. van Willigen, D. J. Stufkens, A. Oskam, *J. Phys. Chem.* **1996**, *100*, 18607.
[9] I. R. Farrell, P. Matousek, C. J. Kleverlaan, A. Vlček, Jr, *Chem. Eur. J.* **2000**, *6*, 1386; I. R. Farrell, A. Vlček, Jr, *Coord. Chem. Rev.* **2000**, *208*, 87.
[10] K. Finger, C. Daniel, *J. Chem. Soc. Chem. Commun.* **1995**, 63; K. Finger, C. Daniel, *J. Am. Chem. Soc.* **1995**, *117*, 12322.
[11] D. Guillaumont, K. Finger, M. R. D. Hachey, C. Daniel, *Coord. Chem. Rev.* **1998**, *171*, 439.
[12] D. Guillaumont, C. Daniel, *Coord. Chem. Rev.* **1998**, *181*, 177.
[13] D. Guillaumont, M. P. Wilms, C. Daniel, D. J. Stufkens, *Inorg. Chem.* **1998**, *37*, 5816.
[14] M. P. Aarnts, D. J. Stufkens, M. P. Wilms, E. J. Baerends, A. Vlček, Jr, I. P. Clark, M. W. George, J. J. Turner, *Chem. Eur. J.* **1996**, *2*, 1556.
[15] M. P. Aarnts, M. P. Wilms, K. Peleen, J. Fraanje, K Goubitz, F. Hartl, D. J. Stufkens, E. J. Baerends, A. Vlček, Jr, *Inorg. Chem.* **1996**, *35*, 5468.
[16] M. P. Aarnts,; M. P. Wilms, D. J. Stufkens, E. J. Baerends, A. Vlček, Jr, *Organometallics* **1997**, *16*, 2055.
[17] D. Guillaumont, C. Daniel, *J. Am. Chem. Soc.* **1999**, *121*, 11733.
[18] B. D. Rossenaar, C. J. Kleverlaan, M. C. E. van de Ven, D. J. Stufkens, A. Oskam, J. Fraanje, K. Goubitz, *J. Organomet. Chem.* **1995**, *493*, 153.
[19] S. G. Kukolich, S. M. Sickafoose, *J. Chem. Phys.* **1993**, *99*, 6465.
[20] M. R. J. Hachey, C. Daniel, *Inorg. Chem.* **1998**, *37*, 1387.
[21] M. C. Heitz, C. Daniel, *J. Am. Chem. Soc.* **1997**, *119*, 8269.
[22] D. Andrae, U. Haeussermann, M. Dolg, H. Stoll, H. Preuss, *Theor. Chim. Acta* **1990**, *77*, 123.
[23] A. Bergner, M. Dolg, W. Kuechle, H. Stoll, H. Preuss, *Mol. Phys.* **1993**, *80*, 1431.
[24] S. Huzinaga, *J. Chem. Phys.* **1965**, *42*, 1293.
[25] MOLCAS 4.1, K. Andersson, M. R. A. Blomberg, M. P. Fülscher, G. Karlström, R. Lindh, P.-Å. Malmqvist, P. Neagrady, J. Olsen, B. O. Roos, A. J. Sadlej, M. Schütz, L. Seijo, L. Serrano-Andrés, P. E. M. Siegbahn, P.-O. Widmark, **1998**, University of Lund (Sweden).
[26] C. Ribbing, C. Daniel, *J. Chem. Phys.* **1994**, *100*, 6591.
[27] K. Finger, C. Daniel, P. Saalfrank, B. Schmidt, *J. Phys. Chem.* **1996**, *100*, 3368.
[28] A. D. Becke, *J. Chem. Phys.* **1993**, *98*, 5648.
[29] T. H. Dunning, Jr., P. J. Hay in *Modern Theoretical Chemistry* (Ed.: H. F. Schaefer, III), Plenum, NY, **1976**, *Vol. 3*, p. 1.
[30] P. J. Hay, W. R. Wadt, *J. Chem. Phys.* **1985**, *82*, 299.
[31] Gaussian 98, Revision A. 7, M. J. Frisch, G. W. Trucks, H. B. Schlegel, G. E. Scuseria, M. A. Robb, J. R. Cheeseman, V. G. Zakrzewski, J. A. Montgomery, Jr., R. E. Stratmann, J. C. Burant, S. Dapprich, J. M. Millam, A. D. Daniels, K. N. Kudin, M. C. Strain, O. Farkas, J. Tomasi, V. Barone, M. Cossi, R. Cammi, B. Mennucci, C. Pomelli, C. Adamo, S. Clifford, J. Ochterski, G. A. Petersson, P. Y. Ayala, Q. Cui, K. Morokuma, D. K. Malick, A. D. Rabuck, K. Raghavachari, J. B. Foresman, J. Cioslowski, J. V. Ortiz, A. G. Baboul, B. B. Stefanov, G. Liu, A. Liashenko, P. Piskorz, I. Komaromi, R. Gomperts, R. L. Martin, D. J. Fox, T. Keith, M. A. Al-Laham, C. Y. Peng, A. Nanayakkara, C. Gonzalez, M. Challacombe, P. M. W. Gill, B. Johnson, W. Chen, M. W. Wong, J. L. Andres, C. González, M. Head-Gordon, E. S. Replogle, J. A. Pople, Gaussian, Inc., Pittsburgh PA, **1998**.
[32] B. Hartke, J. Manz, J. Mathis, *Chem. Phys.* **1989**, *139*, 123; T. Joseph, T. M. Kruel, J. Manz, I. Rexrodt, *Chem. Phys.* **1989**, *139*, 323.
[33] C. C. Marston, G. G. Balint-Kurti, *J. Chem. Phys.* **1989**, *91*, 3571.
[34] H. Tal-Ezer, R. Kosloff, *J. Chem. Phys.* **1984**, *81*, 3967.
[35] G. Katz, R. Baer, R. Kosloff, *Chem. Phys. Lett.* **1995**, *239*, 230.
[36] C. Daniel, D. Guillaumont, C. Ribbing, B. Minaev, *J. Phys. Chem. A* **1999**, *103*, 5766.
[37] S. S. Kristjansdottir, J. R. Norton, in *Transition Metal Hydrides* (Ed.: A. Dedieu), VCH, New York **1991**, pp. 309–359.
[38] W. A. Ehlers, G. Frenking, *Organometallics* **1995**, *14*, 423, and references therein.
[39] I. Bruand-Cote, D. Guillaumont, C. Daniel, unpublished results.

Received: June 15, 2001 [F3337]